RSC Advances

ROYAL SOCIETY OF CHEMISTRY

www.rsc.org/advances

Journal Name

ARTICLE

Dissipative Particle Dynamics Simulation on Morphologies and Dynamics of Linear ABC Triblock Copolymers in Solutions†

Received 00th January 20xx,
Accepted 00th January 20xx

DOI: 10.1039/x0xx00000x

www.rsc.org/

Chun Zhou,[a] Honggang Xia,*[b] Yang Zhou,*[c] Xianggui Xue[c] and Shikai Luo[c]

Due to the great potentialities in the field of multifunctional nanoreactors and carriers, several previous works have shown the interesting morphologies of multicompartment micelles from simple linear ABC triblock copolymers in the dilute solution. In this work, for linear ABC terpolymers, their concentration-induced morphologies and morphological transition are investigated with dissipative particle dynamics simulations. Firstly, several novel morphologies beyond the findings in the dilute solution, including the spherical core-shell-corona (CSC) micelle containing a small reverse CSC inside, the hexagonal packed cylinders in a lamella, the disk CSC micelle with a ring core, the multi-segment with a ring shell, and so on, are observed by varying the terpolymer concentration and the ratio of three blocks. Secondly, the increase of the concentration generally results in the morphological transition from three- or two-dimensional (3D or 2D) to one-dimensional (1D) structures. Finally, the dynamic pathway of morphological formation is similar to that of ABC star mikoarm terpolymers, which has three steps, i.e., nucleation, coalescence and growth. Moreover, the qualitative analysis shows that the interfacial tension play a definite role in the formation of final morphologies. This work enriches the molecular-level knowledge of the morphology of multicompartment micelles from the concentration-induced self-assembly of simple linear ABC terpolymers and reveals their formation pathways, which will be useful for the future preparation and application of novel micelles.

1 Introduction

Exquisitely ordered nanostructures from the self-assembly of block copolymers attracts much attention in the field of drug delivery, microelectronic materials, advanced plastics and so on.[1-4] Precise synthetic methods developed over the past decade afford access to a broad portfolio of multiblock copolymers,[5-7] which offers unparalleled opportunities for designing new nanostructures by the fascinating bottom-up self-assemble strategy. At the same time, it also open the Pandora's Box, myriad molecular design possibilities pose a daunting challenge for experiments, even for theories and simulations.[8] Up to now, the simplest AB diblock copolymer has been investigated most extensively by various means, leading to an in-depth understanding on their self-assemble behaviours.[1] It is well known that, only adding a third block, the ABC triblock copolymer can dramatically expand the spectrum of accessible morphologies and, therefore, are rapidly given more attentions. This kind of terpolymer mainly generate a variety of well-controlled multicompartment micelles with nanosized structural units, originally proposed by Helmut Ringsdorf.[9] Accordingly, in order to know what valuable ABC terpolymers should be synthesized for given applications, understanding the fundamental principles of governing their morphologies on the molecular level are of fundamental importance.

The early studies regarded the concentric (core-shell-corona, CSC) onion morphologies as the default structure adopted by linear ABC (*l*-ABC) triblock copolymers.[10] It brings that, after the pioneer work by Lodge et al,[11] most investigations had been focused on the self-assembly of ABC miktoarm star copolymers (μ-ABC). The main reason is that the miktoarm star copolymer can effectively suppress the concentric onion structure, leading to a fascinating array of new morphologies, such as bowl, worm, hamburger, and raspberry, and so on.[12,13] Especially, a series of simulation and theoretical studies have also been performed to give a molecular-level understanding of the self-assembly of μ-ABC.[14-19] Recently, the works of Laschewsky and co-workers reveal an inspiring result that *l*-ABC terpolymers with different block sequences can also form nonconcentric complex micelles.[20-24] Additionally, depending on the mixtures of THF, water and organic multiacids, Muller and co-workers also found several novel micelles (vesicle, toroid and undulated ribbon) from the self-assembly of *l*-ABC terpolymers.[25] These significant experiments richly testify that the potential of the simple *l*-ABC terpolymer is grossly underestimated. Subsequently, we utilized DPD simulations to explore the phase diagram of *l*-ABC in the dilute solution. Rich

[a] School of Materials Science and Engineering, Southwest University of Science and Technology, 621010 Mianyang, China.
[b] The 1st Affiliated Hospital of Dalian Medical University, 116000 Dalian, China. E-mail: xia_honggang@126.com.
[c] Institute of Chemical Materials, Chinese Academy of Engineering and Physics, 621010 Mianyang, China. E-mail: zhouy@caep.cn.

† Electronic Supplementary Information (ESI) available: all equilibrium micelle morphologies. See DOI: 10.1039/x0xx00000x

complex morphologies beyond the traditional understanding, such as raspberry-onion, helix-on-sphere, cage, ring, bowl, are revealed and two interesting dynamic evolution mechanisms, "contacting and fusing" and "folding and fusing" are also provided.[26,27] Based on DPD simulations, there are other important investigations on the morphologies of linear ABC triblock copolymers in the dilute solutions and blends.[15,16,28,29] In addition, Monte Carlo technique and self-consistent field theory are successfully used to explore the complex self-assemble behaviours of *l*-ABC in the different conditions.[30-32] The continual studies in experiments, simulations and theories enrich our knowledge on the self-assemble behaviours of linear and star ABC triblock copolymers, especially in the dilute solutions. However, for linear ABC terpolymers, the simulation (experimental or theoretical) works focusing on concentration-induced morphologies and morphological transition is still rare. In experiment, the EISA (solvent evaporation induced self-assembly) method has been used to fabricate the template from ABC triblock copolymers.[33] Moreover, our previous DPD simulations also show that, for the rod-coil-rod (ABA) triblock copolymer, the increase of concentration can effectively induce much novel morphologies.[34] Thus, in this work, we again use DPD technique to predict the concentration induced morphologies of *l*-ABC terpolymers with the different block sequences and the block lengths. Furthermore, the dynamic evolution pathways of several new morphologies are also investigated.

2 Method and Model Details

The DPD method, originally developed by Hoogerbrugge and Koelman,[35] is a coarse-grained particle-based dynamics simulation technique, which is similar to MD but allows the simulation of hydrodynamic behaviour in much larger, complex systems, up to the microsecond range. Like MD, DPD particles obey Newton's equation of motion, and the total forces on a particle i include a conservative force $\boldsymbol{F}^C$, a dissipative force $\boldsymbol{F}^D$ and a random force $\boldsymbol{F}^R$, *i.e*,

$$f_i = \sum_{j\neq i}(F_{ij}^C + F_{ij}^D + F_{ij}^R) \qquad (1)$$

The three forces for nonbonded beads are given by

$$\begin{aligned} F_{ij}^C &= -a_{ij}w^C(r_{ij})\mathbf{e}_{ij} \\ F_{ij}^D &= -\gamma w^D(r_{ij})(\mathbf{e}_{ij}\cdot\mathbf{v}_{ij})\mathbf{e}_{ij} \\ F_{ij}^R &= \sigma w^R(r_{ij})\xi_{ij}\Delta t^{-0.5}\mathbf{e}_{ij} \end{aligned} \qquad (2)$$

where α_{ij} is the repulsion parameter between bead i and j, which reflects the chemical characteristics of interacting beads; and $\mathbf{r}_{ij}=\mathbf{r}_i-\mathbf{r}_j$, $r_{ij}=|\mathbf{r}_{ij}|$, $\mathbf{e}_{ij}=\mathbf{r}_{ij}/r_{ij}$ and $\mathbf{v}_{ij}=\mathbf{v}_i-\mathbf{v}_j$. ζ_{ij} is a Gaussian random number with zero mean and unit variance. γ is the friction constant and σ characterizes the noise strength. For ensuring the system to satisfy the fluctuation-dissipation theorem and correspond to the Gibbs Canonical ensemble, only one of the two weight functions w^D and w^R can be chosen arbitrarily and this choice fixes the other one.[36] There is also a relation between the amplitudes (σ and γ) and k_BT. It is $w^D=(w^R)^2$ and $\sigma^2=2\gamma k_BT$, where k_B is the Boltzmann constant and T is the temperature. Generally, based on the work of Groot and Warren,[37] the simple form for $w^D=(w^R)^2=(1-r_{ij})^2$ and $\sigma=3(\gamma=4.5)$ are used, and Newton equations for all beads are integrated by a modified version of the velocity-Verlet algorithm with $\lambda=0.65$. The particles connected by the spring force can be used to represent a polymer, and the interaction force $\boldsymbol{F}^S$ for bonded beads is

$$F_{ij}^S = -\sum_{j\neq i} k_S(l_{ij}-l_0) \qquad (3)$$

where l_{ij} is the bond length between connected two bead i and j. Here, the spring coefficient $k_S=4$ and the balance bond length $l_0=0$ are chosen. For easy numerical handling, the cutoff radius r_c, the bead mass m, and the temperature k_BT are chosen as the unit of the simulated system.

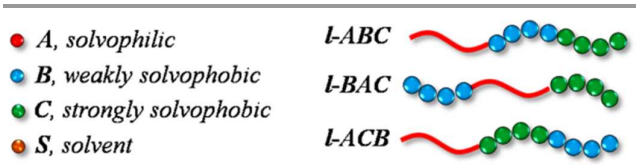

Fig. 1 The coarse-grained model of the linear ABC triblock copolymer with different block sequences.

Table 1 Repulsion parameters (DPD unit) in this work

	A	B	C	S
A	25	45	90	27
B	45	25	75	50
C	90	75	25	120
S	27	50	120	25

Figure 1 gives our coarse-grained models for *l*-ABC (*x*-*y*-*z*), *l*-BAC (*y*-*x*-*z*) and *l*-ACB (*x*-*z*-*y*) are consisted of the solvophilic block (A), the weakly solvophobic block (B) and the strongly solvophobic block (C), *x*, *y* and *z* are the number of bead A, B and C, respectively. The solvent is represented by an individual bead *S*. The interaction parameters chosen are listed in Table 1. In fact, these appropriate DPD parameters firstly defined by Zhong *et al* to describe the multicompartment micelles of the famous *u*-EOF miktoarm terpolymer.[14] The subsequent DPD simulations also used the same parameters and successfully explored the morphological diversity of ABC terpolymer systems.[15] However, Sheng *et al* think that the interactions between the poly(perfluoropropylene oxide) (F) block and other two blocks are very strong and provide a suite of gentle parameters.[16] Here, our main aim is to obtain the universal rule of governing concentration-induced morphologies for *l*-ABC in solutions. Therefore, we still adopt these present parameters for better comparison with our previous works.

To avoid the finite size effect, our simulations are performed in a larger cubic box of size $(30r_c)^3$ under periodic boundary, containing 81000 DPD beads with random distribution at $\rho=3$. The concentrations (φ, represented by the volume fraction of

terpolymers) of *l*-ABC in solutions are chosen at the range of 0.05-0.3 for checking the efficacy of varied concentrations. The time step Δt is 0.05 and a total of 1~2×10^6 DPD time steps are carried out to guarantee the equilibration for each system.

3 Results and Discussion

In general, the morphology of ABC triblock copolymers in the solvent is influenced by the concentration, the block length (or ratio), the interaction between different compositions, and so on. This is a large parameter space. It is difficult to consider all the factors influencing the morphology. In the present work, we fixed all the interaction parameters as listed in Table 1 and focused on the effect of varied concentration (φ) and the block length (by varying *x*, *y* and *z*) on the morphologies and their dynamics evolutions. For one of three sequences (*l*-ABC, *l*-BAC and *l*-ACB), there are 7 kinds of linear terpolymers with the different block length (2-2-2, 2-2-8, 2-8-2, 8-2-2, 2-8-8, 8-2-8, 8-8-2), 6 kinds of concentrations (φ=0.05, 0.1, 0.15, 0.2, 0.25, 0.3) and is a total of 42 combinations. Considering all three sequences, a total of 126 equilibrium micellar morphologies (see ESI) are provided by our simulations. Several novel morphologies, not found by the self-assembly in the dilute solutions (generally φ=0.1), are provided firstly. Next, we will introduce these new morphologies and their dynamics evolutions according to the order of *l*-BAC, *l*-ABC and *l*-ACB in detail.

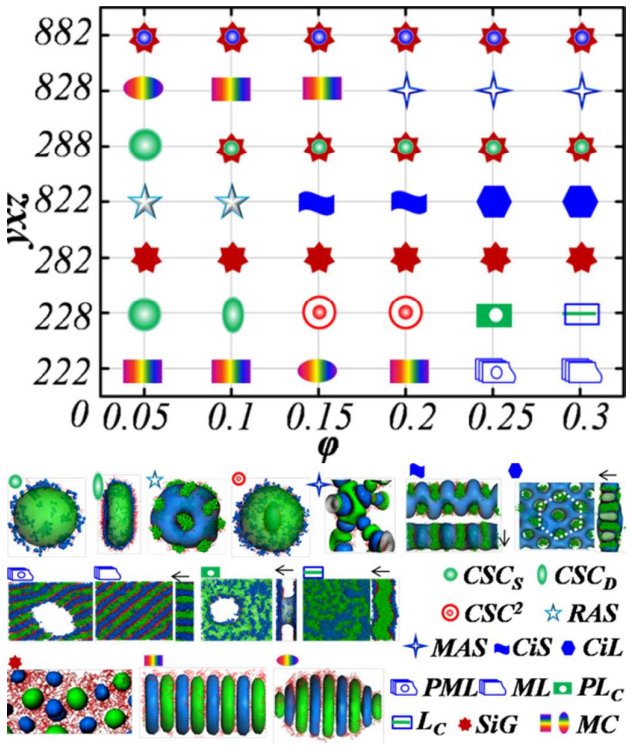

Fig. 2 Top, the morphological phase diagram of *l*-BAC terpolymers in solutions. The three numbers listed in y-axis is *yxz*, which represents the length of block B, A and C, respectively. φ of x-axis is the concentration of *l*-BAC. Down, simulation morphologies represented by the symbols in phase diagram. Red, blue and green represents A-, B- and C-rich domains, respectively. For clarity, several morphologies use the isodensity surface. CSC$_S$ and CSC$_D$, spherical and disk core-shell-corona (CSC) micelle, respectively. CSC^2, a big CSC micelle containing a small CSC inside. RAS, raspberry micelle. MAS, multi-arm segment. CiS, cylinder in strip. CiL, cylinder in lamella. PML, perforated multi-layer. ML, multi-layer. PL$_C$, perforated lamella with a middle of block C. L$_C$, lamella with a middle of block C. SiG, sphere in gel. MC, multicore.

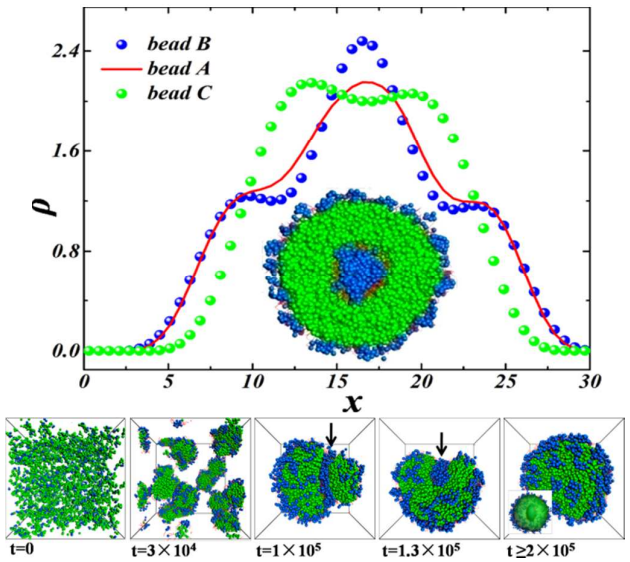

Fig. 3 Top, the density profile in z direction for CSC^2 micellar morphology and the inline image is the cutting image. Down, the dynamic evolution of the CSC^2 micelle. Red, blue and green represents A-, B- and C-rich domains, respectively.

For *l*-BAC, the middle solvophilic block (A) as a bridge links two solvophobic blocks (B and C). The terpolymers with this kind of block sequence can bring more novel morphologies than other two block sequences (introduced in the following text). Figure 2 gives the phase diagram and detailed morphologies of *l*-BAC as a function of the block length (*y*-*x*-*z*) and the concentration (φ), respectively. As shown in Figure 2 (top), the common core-shell-corona micellar structures (CSC$_S$ and CSC$_D$) rarely appear in the whole phase space. A new CSC morphology, CSC^2, is revealed for *l*-BAC (2-2-8) at φ=0.15 and 0.2. Our previous simulations[26,27] missed this interesting micellar morphology because of the low concentration (φ=0.1). To carefully examining the internal structure of CSC^2, we give its density profile and the cutting image in Figure 3 (top). The density profile shows that, under $\rho\approx$1.2, blocks A and B form a shell surrounding block C. However, beyond $\rho\approx$1.2, blocks A and B hide in block C. Based on the sunken degree of ρ of bead C, we can deduce the formation of a small inner core. Due to the spherical symmetry, the other two density profiles in x and y direction have the similar result, and we don't show and discuss them again. Combining the cutting image of CSC^2, we can find that the outer-portion is a natural CSC structure, *i.e.* B is a shell and C is a core. However, the inner is a reversed CSC, *i.e.* C is a shell and B is a core (A always locates in the interface of B and C domains). Only considering the thermodynamic factor, it is obvious that the interaction between the block and the solvent drive the formation of the outer-portion, and the interaction among the blocks bring the inner one. For an in-depth understanding, we also investigate the dynamics

evolution of CSC^2 micelle and the result is given in Figure 3 (down). It is easy to know that the shorter solvophilic B block make the system unstable and several droplets with the common CSC structure are formed at a short time ($t=3\times10^4$). After that, the neighbouring droplets coalescence and become more and more big with the increase of time. At the latter stage, once a larger micelle contacts with other one ($t=1\times10^5$), both blocks A and B get together at the contacted interface (see the arrows labelled in Figure 3) and then are embedded in the interior by the fusing of block C. The result indicates that the formation of structure follows the four steps, which are of nucleation, coalescence, growth and embedding. If the latter stage (after $t=1\times10^5$) is broken by the dynamic method, the common CSC, not the novel CSC^2 structure, would be obtained. Therefore, we can know that controlling the dynamic evolution pathway is also a good alternative to tune the different morphologies for *l*-BAC terpolymers in solutions. In experiment, Cui and co-workers had used divalent organic counter ions and solvent mixtures to drive the organization of block copolymers down the specific dynamic pathway into complex one-dimensional structures.[38]

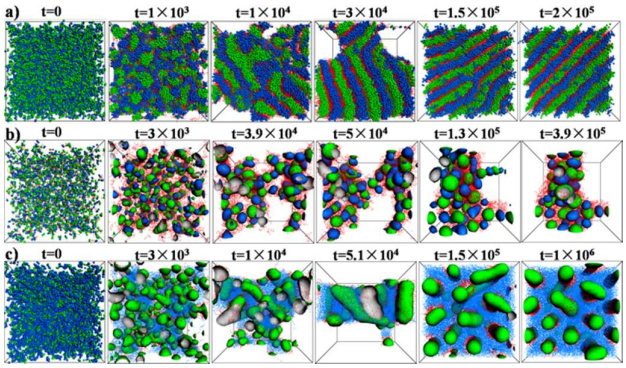

Fig. 4 Dynamic evolution of ML (a), SiG (b) and CiL (c) micelles, respectively. Red, blue and green represents A-, B- and C-rich domains, respectively. For clarity, B and C-rich domains for SiG and C-rich domains for CiL morphologies use the isodensity surface, respectively.

Figure 4 gives the dynamic evolution of other three interesting morphologies, which are ML, SiG and CiL, respectively. As for ML (representing multi-layer structure) of *l*-BAC (2-2-2) at φ=0.3, alternate solvophobic blocks B and C (layers) linked by the solvophilic block A form a one-piece lamella with a thickness of about 15 DPD unit, and the thickness of single layer (B or C) is about a third of the lamella. The evolution of ML structure in Figure 4a shows that discrete blocks B and C-rich domains come forth firstly, and then individually fuse into the continuous rich domains. Finally, the whole evolves into a lamella. When the concentration decreases to φ=0.25, the perforated multi-layer (PML) can be formed. SiG (sphere in gel) is that blocks B and C assemble the unattached spheres distributing in the gels of block A. *l*-BAC terpolymers with longer solvophilic block A prefer to form this kind of structure and the different ratio of block B and C would result in the different spherical size. For example, the ratio of B to C in *l*-BAC (8-8-2) is 4, which brings the bigger blue spheres of block B and the smaller green spheres of block C in the red gels of block A (see ESI). As shown in Figure 4b, the formation of SiG morphology has only two steps, nucleation and growth. In despite of the simple dynamic formation pathway, the gelation behaviour of ABC terpolymers[39] and its application in the drug release[40] have been given more and more attention. Then, the other interesting CiL (cylinder in lamella) structure from *l*-BAC (8-2-2) at high concentration φ=0.3 is that the hexagonal packed cylinders of block C set in the lamella of block B, and the two domains are linked by the block A. However, at low concentrations φ=0.05 and 0.1, *l*-BAC (8-2-2) triblock copolymer forms the raspberry-like (RAS) morphology. By comparing, we can find the obvious effect of concentration on the morphology again. Figure 4c gives the formation pathway of CiL morphology. The result shows that block C firstly arise the nucleation in the gel of block B at early stages ($t=3\times10^3$), then coalescence and growth. At the same time, the shape of the whole shape develops into the lamella ($t=5.1\times10^4$). When the lamella is stable, the block C maintain the trend of evolution (coalescence and growth) and begin to show the cylindrical shape ($t=1.5\times10^5$), up to the formation of hexagonal packing ($t=1\times10^6$). In fact, the dynamic evolution of RAS morphology is very different with the above one due to the different concentration, which follows the mechanism of "contacting and fusing" from the small raspberry nucleation.[27] Therefore, the concentration increase of ABC terpolymers in solutions can not only influence the final morphology but also the dynamic pathway.

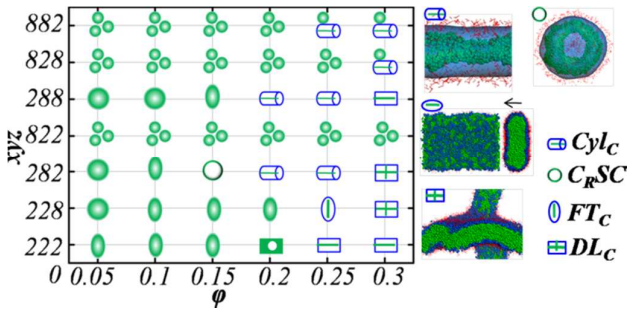

Fig. 5 Left, the morphological phase diagram of *l*-ABC in solutions. *xyz* in y-axis represent the length of A, B and C, respectively. Right, simulation morphologies represented by the symbols in phase diagram. Cyl_C, cylindrical CSC micelle with a core of block C. C_RSC, disk CSC micelle with a ring core of block C. FT_C, flat tube CSC structure with a core of block C. DL_C, distorted lamella with a middle of block C. Three green spheres represent the congeries of several single CSC micelles. Red, blue and green represents A-, B- and C-rich domains, respectively. For clarity, B-rich domains in partial snapshots use the isodensity surface.

For *l*-ABC, the solvophilic block A orderly links the weakly solvophobic block B and the strongly solvophobic block C. The terpolymers with this sequence generally form large numbers of concentric CSC morphologies, as shown in Figure 5. In the left phase diagram, it is mainly occupied by the typical spherical and disk CSC micelles, which are the core of block C, the shell of block B and the corona of block A, and are represented by green sphere, especially at low concentrations. Here, we don't distinguish the spherical CSC morphologies as our previous work based on their different shells, which can

adopt several interesting morphologies, such as ring, cage, and helix.[26] In addition, several new morphologies (C_RCS, Cyl_C, FT_C and DL_C) driven by the high concentration are still found, which also testify the effect of concentration on the morphology. When the solvophilic block A is enough long, such as *l*-ABC terpolymers (8-2-2, 8-2-8 and 8-8-2), they prefer to form the absolute small CSC micelles and get together like the gel (the symbol is three sphere in Figure 5), however, which is different from the SiG morphology from *l*-BAC (2-8-2, 2-8-8 and 8-8-2). The obvious difference is that we can draw out an integrated CSC micelle from the above gels and not obtain anything from SiG gels.

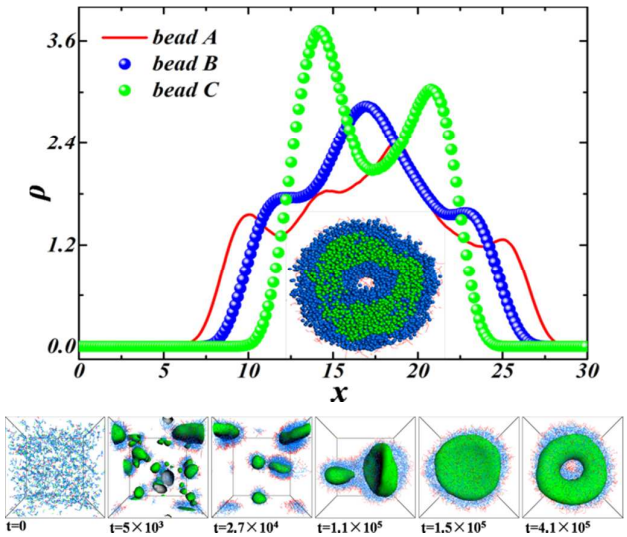

Fig. 6 Top, the density profile for C_RSC micellar morphology and the inset image is the cutting image. Down, the dynamic evolution of C_RSC micelle. Red, blue and green represent A-, B- and C-rich domains, respectively. For clarity, C-rich domains use the isodensity surface.

In addition, it is interesting that the new C_RSC (disk CSC micelle with a ring core of block C) micelle is firstly detected for *l*-ABC (2-8-2) at φ=0.15. Figure 6 (top) shows the internal structure of C_RSC micelle based on its density profile and the section image along the longest diameter. The ρ data of bead C appears an obviously decrease in the structural middle. Combining the cutting image, we can clearly know that the ring structure of block C result in the valley of ρ data. The raised peak of ρ data for bead A and B indicates that a number of beads A and B concentrate in the central hole of the C ring. Additionally, the cutting image shows a small hole in the centre of the whole micelle, which testify that the whole C_RSC is also a ring structure. For exploring the formation of C_RSC micelle, we also simulate its dynamics evolution pathway, as shown in Figure 6 (down). Before t=1.5×10^5, the *l*-ABC (2-8-2) terpolymer has the same evolution, i.e. nucleation of block C, coalescence and growth, as several *l*-ABC terpolymers with the disk-like CSC morphology (CSC_D). However, the transformation from CSC_D to C_RSC is a direct process without a transition state. It is a pity that we don't find out the direct reason of this process. An apparent explanation is that the ring structure of C_RSC is to ensure the biggest contacting area between the solvent S and the solvophilic block A. Of course, by the shape variation from an integrated disk to a ring, we can speculate a qualitative change of interfacial tension for the micelle. Though the interfacial tension for planar interfaces can be calculated by the pressure tensor with the definition of Irving and Kirkwood,[42-44] that for curving interfaces is still not simulated exactly. To date, therefore, we can only give a qualitative estimation that the interfacial tension is important to drive the dynamic evolution of the micelle from the self-assembly of ABC terpolymers.

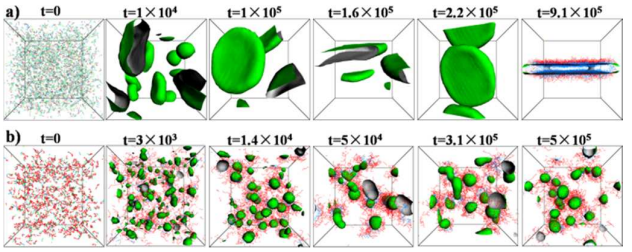

Fig. 7 Dynamic evolution of PL_C (a) and the congeries of CSC micelles (b), respectively. Red, blue and green represent A-, B- and C-rich domains, respectively. For clarity, C-rich domains use the isodensity surface.

From the phase diagrams, we can see that, at high concentrations, linear ABC triblock copolymers are generally inclined to form the lamella morphology including PL_C (perforated lamella with a middle of block C), L_C (lamella with a middle of block C) and DL_C (distorted lamella with a middle of block C), which are very different from the above PML and ML morphologies. They are the normal three-layer lamella, i.e. the strong solvophobic block C in the middle, the weakly solvophobic block B in the two sides and the solvophilic block A in the outsides. This kind of array is easy to understand from the thermodynamic angle, therefore, we further focus on their dynamic pathway and the result is given in Figure 7a. Taking PL_C from *l*-ABC (2-2-2) at φ=0.2 as an example, it is interesting to see a similar formation pathway with C_RSC from *l*-ABC (2-8-2) at φ=0.15. They all firstly form the CSC_D structure by the process of nucleation, coalescence and growth of block C before a given time (here, it is t=2.2×10^5 for PL_C). For PL_C, in the following process, the larger CSC_D micelle turns into a lamella structure through the edge fracture of the integrated disk core (block C) and shell (block B). Obviously, the last morphological transformation should also be ascribed to the influence of interfacial tension. In addition, we also check the dynamics evolution of the congeries of CSC micelles in Figure 7b. The simulation result shows that there are three common steps during the formation of congeries no matter how the concentration, which are nucleation, coalescence and growth. When the single CSC micelle arrives at a given size, the growth is over. The reason is that the longer solvophilic A has enough ability to better screen the influence of the solvent on solvophobic blocks B and C, which contributes to the stable gel-like systems.

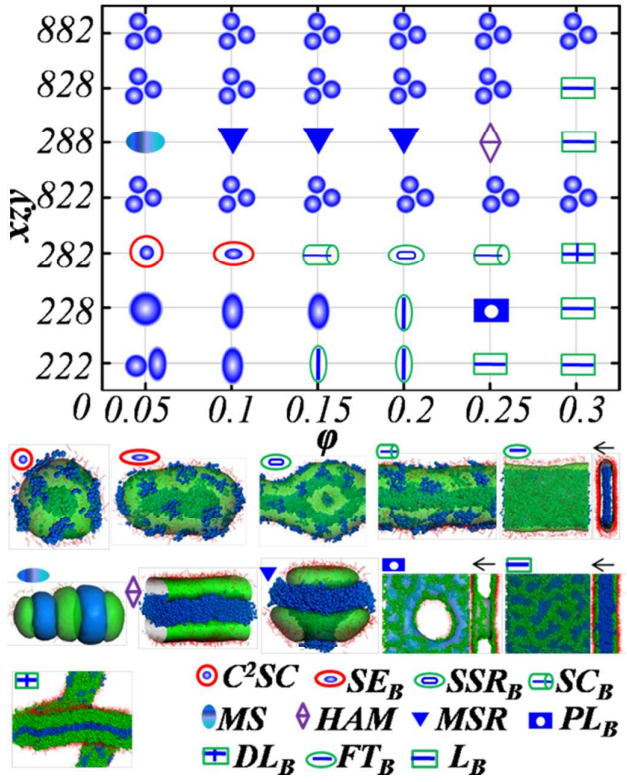

Fig. 8 Top, the morphological phase diagram of *l*-ACB in solutions. *xzy* in y-axis represent the length of A, C and B, respectively. Down, simulation morphologies represented by the symbols in phase diagram. C^2SC, spotted CSC micelle with a core of block B. SE_B, spotted ellipsoid with a core of block B. SSR_B, spotted strip with a ring core of block B. SC_B, spotted cylinder with a core of block B. MS, multi-segment. HAM, hamburger. MSR, MS with a ring segment. PL_B, perforated lamella with a middle of block B. DL_B, distorted lamella with a middle of block B. FT_B, flat tube CSC structure with a core of block B. L_A, lamella with a middle of block B. Red, blue and green represent A-, B- and C-rich domains, respectively.

Compared with *l*-ABC, *l*-ACB merely exchange the sequence of the weakly solvophobic block B and the strongly solvophobic block C. Therefore, like *l*-ABC, the phase diagram (Figure 8, top) of *l*-ACB is dominated by the typical spherical and disk CSC micelle (blue), especially at low concentrations. The only difference is that the cores here are composed of block B (blue sphere). It is clear that *l*-ACB (8-2-2, 8-2-8 and 8-8-2) with longer solvophilic A still prefer to form the congeries of CSC micelles (labelled by three sphere in Figure 8) as same as *l*-ABC terpolymers. At high concentrations, *l*-ACB terpolymers are also inclined to the normal three-layer lamella, i.e. PL_B, L_B and DL_B (block B in the middle) similar to PL_C, L_C and DL_C (block C in the middle) in appearance. Hereinbefore, we have shown the characteristic and the dynamic evolution pathway for these morphologies, and compared with those from *l*-BAC. Here, we don't come again. In fact, the little alternation in the block sequence still brings several different morphologies. For example, *l*-ACB (2-8-2) with longer strong solvophobic block C forms a series of spotted CSC micelles, and the increase of concentrations decides the different shape transition of micelles (from sphere, ellipsoid, cylinder to strip, see Figure 8 down). Among them, the spherical C^2SC micelle is apparently similar to the above spherical CSC^2 micelle. However, by careful comparisons, we distinguish that they have an entirely different kernel. The core of C^2SC only comprise block B, and that of CSC^2 is a reversed CSC containing the three blocks. In addition, the *l*-ACB (2-8-8) at φ=0.1~0.2 forms an interesting MSR morphology, which is that block C builds a round segment ringing the segment of block B. Interestingly, it is in accord with the morphology of laterally structured vesicle with a core from ABC miktoarm star terpolymers found by Wang et al.[41] They have also given its formation pathway including three steps (i.e. nucleation, coalescence and growth).

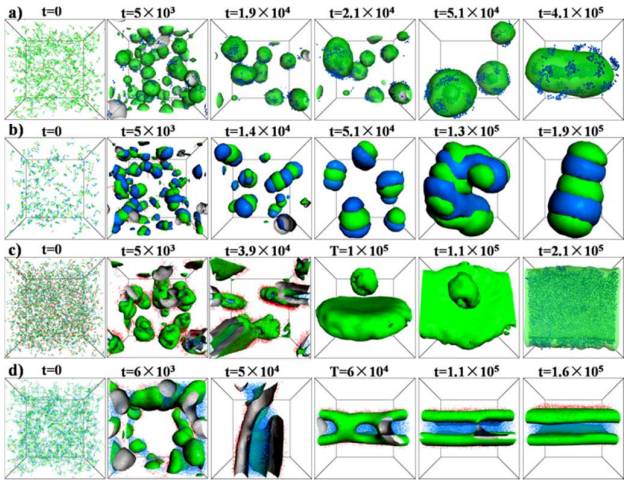

Fig. 9 Dynamic evolution of SE_B (a), MS (b), FT_B (c) and HAM (d) morphologies, respectively. Red, blue and green represent A-, B- and C-rich domains, respectively. For clarity, B and C-rich domains in several snapshots use the isodensity surface.

In order to give insight into these special morphologies, their formation pathways are investigated and given in Figure 9. Firstly, SE_B (spotted ellipsoid with a core of block B) micelle from *l*-ACB (2-8-2) at φ=0.1 is taken as an example to represent the dynamic evolution of the series of spotted CSC micelles. Figure 9a clearly shows that the *l*-ACB (2-8-2) system quickly forms the small CSC micelles in the short time ($t=5\times10^3$), which have the core of block C and the spotted shell of block B. In the following process, the coalescence of CSC micelles makes several separate shells of block B into the core interior of block C and becomes the central deep-seated core. The same dynamic pathway is also found for the raspberry-onion-like micelle of *l*-ABC (2-12-2) at φ=0.1 in our previous work.[27] Finally, the spherical CSC micelles gradually develop into the larger elliptic SE_B micelle by the coalescence. As a whole, the micelles with the inner core can be gained from all linear ABC triblock copolymers with three sequences by the appropriate parameters. It is noteworthy that the tuning of dynamic evolution pathway is one of these important factors. Figure 9b gives the dynamic evolution of the multi-segment (MS) worm-like micelle, whose morphology is close to the MC micelles from *l*-BAC (2-2-2) at φ=0.05 and 0.1. However, there is a little discrepancy between these two morphologies. The alternate B and C disks in MC are separated and also linked by the block A, however, those in MS are directly linked together

and block A distributes the surface of block C as a corona. We have revealed the interesting dynamic pathway of "folding and fusing" for the MC micelle. Here, the dynamic evolution pathway for MS micelle shows a difference, which experiences the nucleation of solvophobic blocks, the coalescence by the "head-to-head" and "shoulder-to-shoulder" fashions, and the final multi-segment (MS) worm-like micelle. Like *l*-ABC (2-2-8) at φ=0.25, all *l*-ACB (2-2-2) at φ=0.15, 0.2 and (2-2-8) at φ=0.2 form the flat tube (FT) CSC structure. The only difference is that the former has a core of block C (FT_C) and the latter has a core of block B (FT_B). The formation pathway of FT_B from *l*-ACB (2-2-8) at φ=0.2 is shown in Figure 9c. From the appearance, we generally think that this kind of flat tube morphology should be from the cylindrical CSC structures, only by a simple extrusion. Interestingly, before the final flat tube structure, it also forms the disk-like CSC structure ($t=1\times10^5$) as same as the C_RSC and PL_C. Obviously, the interfacial tension plays a crucial function during the last transformation of these morphologies. In Figure 9d, we can also see the significant effect of interfacial tension on the formation of the hamburger (HAM) micelle from *l*-ACB (2-8-8) at φ=0.25. The former steps, nucleation and coalescence, don't show the particularity. It should be noticed that a flat tube CSC structure appears at $t=1.1\times10^5$, the difference is that the tube has several holes. With the increase of simulation time, the thin sides of the flat tube disappear and the shape of long hamburger morphology appears gradually. Through more equilibrium time, HAM micelle would achieve at the final stable. In a word, during the dynamic evolution process of the concentration induced self-assembly for linear ABC triblock copolymers, the interfacial tension plays a vital role to decide the final morphology.

4 Conclusions

In summary, based on our previous works, we further utilize DPD simulation method to give insight into the concentration induced self-assemble morphologies of linear ABC triblock copolymers and their dynamic evolution pathway, where A is a solvophilic block, B and C are weakly solvophobic and strong solvophobic blocks, respectively. The concentration (described by the volume fraction, φ) has a remarkable influence on the morphologies and dynamic evolution of micelles. The detail phase diagrams show that, except for the conventional concentric core-shell-corona and other interesting micelles found in the previous works, several novel morphologies beyond the knowledge in the dilute solution are found, such as CSC^2, CiL, ML (or PML), SiG, C_RSC, $FT_{C\ or\ B}$, SSR_B, MSR, $L_{B\ or\ C}$, and so on. In general, with the increase of the concentration, the morphologies change from spherical (three-dimensional, 3D) and multi-layer worm-like, cylindrical or flat tube-like (two-dimensional, 2D), to lamella (one-dimensional, 1D) structures. Furthermore, the formation pathways of several novel structures are analyzed and a universal mechanism with three steps, which are nucleation, coalescence and growth, can be found. In detail, for three typical C_RSC (3D to 2D), FT_B (2D) and PL_C (1D) morphologies, a kind of similar concentric disk-like CSC structure is found in their dynamic stage of growth. Based on the evolution of the whole shape, we can estimate that the interfacial tension plays a significant function in the final formation of morphologies. These results are helpful to understand the formation mechanism of complex multicompartment micelles by the concentration induced self-assembly of linear ABC triblock copolymers and assisting experiments to find new morphologies.

Acknowledgements

All the authors appreciate very much the financial support from Foundation of CAEP (No.2014B0302040, 2014-1-075) and National Nature Sciences Foundation of China (No.11402241).

Notes and references

1 I. W. Hamley, *Block Copolymers in Solution: Fundamentals and Applications*; Wiley: Hoboken, NJ, 2005.
2 M. R. Savic, L. Luo, A. Eisenberg and D. Maysinger, *Science,* 2003, **300**, 615.
3 R. Ruiz, H. Kang, F. A. Detcheverry, E. Dobisz, D. S. Kercher, T. R. Albrecht, J. J. de Pablo and P. F. Nealey, *Science,* 2008, **321**, 936.
4 F. S. Bates, G. H. Fredrickson, D. Hucul and S. F. Hahn, *AIChE J.,* 2001, **47**, 762.
5 C. J. Hawker and K. L. Wooley, *Science,* 2005, **309**, 1200.
6 M. K. Kiesewetter, E. J. Shin, J. L. Hedrick and R. M. Waymouth, *Macromolecules,* 2010, **43**, 2093.
7 K. Okamoto and C. K. Luscombe, *Polymer Chem.,* 2011, **2**, 2424.
8 F. S. Bates, M. A. Hillmyer, T. P. Lodge, C. M. Bates, K. T. Delaney and G. H. Fredrickson, *Science,* 2012, ***336***, 434.
9 H. Ringsdorf, P. Lehmann, R. Weberskirch, Multicompart-mentation - a concept for the molecular architecture of life. In *217th ACS National Meeting*, Anaheim, CA, 1999.
10 N. Hadjichristidis, H. Iatrou, M. Pitsikalis, S. Pispas and A. Avgeropoulos, *Prog. Polym. Sci.*, 2005, **30**, 725.
11 Z. Li, E. Kesselman, Y. Talmon, M. A. Hillmyer, and T. P. Lodge, *Science*, 2004, **306**, 98.
12 A. O. Moughton, M. A. Hillmyer and T. P. Lodge, *Macromolecules*, 2012, **45**, 2.
13 A. Laschewsky, *Curr. Opin. Colloid Interface Sci.*, 2003, **8**, 274.
14 J. Xia and C. Zhong, *Macromol. Rapid Commun.,* 2006, **27**, 1110.
15 Y. Zhao, Y. T. Liu, Z. Y. Lu and C. C. Sun, *Polymer*, 2008, **49**, 4899.
16 S. H. Chou, H. K. Tsao and Y. J. Sheng, *J. Chem. Phys.*, 2006, **125**, 194903.
17 E. B. Zhulina and O. V. Borisov, *Macromolecules*, 2008, **41**, 5934.
18 W. Kong, B. Li, Q. Jin, D. Ding and A. C. Shi, *J. Am. Chem. Soc.*, 2009, **131**, 8503.
19 S. Li, Y. Jiang and J. Z. Y. Chen, *Soft Matter*, 2013, **9**, 4843.
20 M. Kubowicz, J. F. Baussard, J. F. Lutz, A. F. Thunemann, H. von Berlepsch and A. Laschewsky, *Angew. Chem., Int. Ed.*, 2005, **44**, 5262.
21 H. von Berlepsch, C. Bottcher, K. Skrabania and A. Laschewsky, *Chem. Commun.*, 2009, **17**, 2290.
22 K. Skrabania, A. Laschewsky, H. von Berlepsch and C. Bottcher, *Langmuir*, 2009, **25**, 7594.
23 K. Skrabania, H. von Berlepsch, C. Bottcher and A. Laschewsky, *Macromolecules*, 2010, **43**, 271.
24 J. N. Marsat, M. Heydenreich, E. Kleinpeter, H. von Berlepsch, C. Bottcher and A. Laschewsky, *Macromolecules*, 2011, **44**, 2092.

25 E. Betthausen, C. Hanske, M. Müller, A. Fery, F. H. Schacher, A. H. E. Müller, and D. J. Pochan, *Macromolecules,* 2014, **47**, 1672.
26 Y. Zhou, H. G. Xia, X. P. Long, X. G. Xue and W. Qian, *Macromol. Theory Simul.,* 2015, **24**, 85.
27 Y. Zhou, X. P. Long, X. G. Xue, W. Qian and C. Y. Zhang, *RSC Adv.*, 2015, **5**, 7661.
28 L. Wang and J. P. Lin, *Soft Matter*, 2011, **7**, 3383.
29 J. Xin, D. Liu and C. L. Zhong, *J. Phys. Chem. B,* 2009, **113**, 9364.
30 U. Nagpal, F. A. Detcheverry, P. F. Nealey, and J. J. de Pablo. *Macromolecules,* 2011, **44**, 5490.
31 Y. T. Zhu, X. P. Yang, W. X. Kong, Y. P. Sheng and N. Yan, *Soft Matter*, 2012, **8**, 11156.
32 L. Q. Wang and J. P. Lin, *Soft Matter*, 2011, **7**, 3383.
33 J. Y. Zhang, Y. H. Deng, J. Wei, Z. K. Sun, D. Gu, H. Bongard, C. Liu, H. H. Wu, B. Tu, F. Schuth, and D. Y. Zhao, *Chem. Mater.,* 2009, **21**, 3996.
34 Y. Zhou, S. Song, X. P. Long, C. Y. Zhang and Y. M. Chen, *Macromol. Theory Simul.,* 2014, **23**, 490.
35 P. J. Hoogerbrugge, *Europhys. Lett.*, 1992, **19**, 155.
36 P. Español and P. B. Warren, *Europhys. Lett.,* 1995, **30**, 191.
37 R. D.Groot and P. B. Warren, *J. Chem. Phys.*, 1997, **107**, 4423.
38 H. G. Cui, Z. Y. Chen, S.Zhong, K. L. Wooley and D. J. Pochan. *Science*, 2007, **317**, 647.
39 C. Zhou, M. A. Hillmyer, and T. P. Lodge, *J. Am. Chem. Soc.,* 2012, **134**, 10365.
40 M. K. Gupta, J. R. Martin, T. A. Werfel, T. W.Shen, J. M. Page, and C. L. Duvall, *J. Am. Chem. Soc.,* 2014, **136**, 14896.
41 L. Wang, R. Xu, Z. L. Wang and X. H. He, *Soft Matter*, 2012, **8**, 11462.
42 J. H. Irving and J. G. Kirkwood, *J. Chem. Phys.,* 1950, **18**, 817.
43 H. J. Qian, Z. Y. Lu, L. J. Chen, Z. S. Li and C. C. Sun, *J. Chem. Phys.,* 2005, **122**, 184907.
44 Y. Zhou, X. P. Long and Q. X. Zeng, *Polymer*, 2011, **52**, 6110.

